Nanoscale

COMMUNICATION

View Article Online
View Journal | View Issue

Cite this: *Nanoscale*, 2015, **7**, 9153

Received 12th January 2015,
Accepted 17th April 2015

DOI: 10.1039/c5nr00242g

www.rsc.org/nanoscale

Well-oriented epitaxial gold nanotriangles and bowties on MoS_2 for surface-enhanced Raman scattering†

Haiqing Zhou,‡[a,b] Fang Yu,‡[a,b] Chuan Fei Guo,[a] Zongpeng Wang,[c] Yucheng Lan,[a] Gang Wang,[b] Zheyu Fang,[c] Yuan Liu,[a] Shuo Chen,[a] Lianfeng Sun*[b] and Zhifeng Ren*[a]

We report on epitaxial growth of Au nanotriangles (AuNTs) and bowties consisting of opposing tip-to-tip AuNTs with a few-nanometer gap on *n*-layer MoS_2. These AuNTs exhibit well-defined crystallographic orientations with the average size determined by the MoS_2 thickness. Monolayer (1L) MoS_2 shows the weakest coalescence, corroborating the layer-dependent interactions among Au and *n*-layer MoS_2. High-resolution transmission electron microscopy characterization confirms the lattice directing of thin MoS_2 sheets on the AuNT formation with $[111]_{Au}||[001]_{MoS_2}$ and $<211>_{Au}||<210>_{MoS^2}$. By introducing misfit dislocation arrays, the system with an 8.8% lattice misfit is stress-free. In particular, subwavelength-sized gold bowtie nanoantennas can be easily found on the MoS_2 surface with a spacing gap down to 3 nm and a density up to 1.6×10^{13} m^{-2}. This technique is low cost, time-saving and free of impurities compared to the conventional lithography technologies. Meanwhile, the equilateral AuNTs can enhance Raman signals of thin MoS_2 sheets far stronger than that by ordinary gold films, indicating the potential use of AuNTs as SERS substrates for SERS applications.

Introduction

Since the discovery of graphene in 2004,[1] considerable efforts have been devoted to two-dimensional layered materials.[2–4] With the thickness of a layered material reduced to nanoscale, the electronic, magnetic, optical and chemical properties may undergo remarkable changes depending on the number of layers, which are obviously different from its bulk counterpart. For example, with reduced number of layers, size effects have been observed on surface diffusion of metal adatoms on graphene.[5–7] For *n*-layer MoS_2, it has a tunable bandgap as the number of layers (thickness) decreases, and monolayer MoS_2 becomes a direct band-gap semiconductor in contrast to few-layer or bulk MoS_2 with indirect bandgaps.[8] In particular, a single layer of MoS_2 can be divided into three weakly bonded S–Mo–S layers with one S layer at the surface through van der Waals force, which is suitable for metal adsorption and binding.[9,10] Furthermore, the growth and anisotropic etching of MoS_2 single crystals usually exhibit triangular shapes.[11–13] Thus, due to its single crystalline nature, it is intuitive to imagine that two dimensional layered MoS_2 can be used as templates for the growth of single crystalline epilayers or crystallographically oriented nanostructures. Although significant efforts have been devoted to investigating the electronic and optical properties of layered MoS_2 and its synthesis,[8,11,14,15] evaluating layered MoS_2's potential usefulness for epitaxial growth is still in its infancy.[16]

Nowadays, the controlled synthesis of AuNTs is of particular interest because of their potential use in cancer hyperthermia, plasmonic nanoantennas,[17] surface enhanced Raman scattering (SERS),[18] *etc*. Usually, it is essential to assemble them on planar surfaces for many sensing and catalytic applications, which is achieved by post treatment after solution-phase synthesis.[19,20] In this sense, it is highly desirable to realize the simultaneous growth and assembly of AuNTs without introducing any reagents in the experiments. On the other hand, subwavelength-sized gold bowtie nanoantennas, consisting of two opposing tip-to-tip AuNTs separated by a small gap, have attracted great attention due to their applications in SERS or fluorescence,[21] optical imaging and storage, molecular sensing,[22] *etc*. It is suggested that an extremely high electromagnetic field enhancement can be achieved within the gap and confined to the area near the gap due to the coupled plasmon resonance between two AuNTs, which would serve as

[a]*Department of Physics and TcSUH, University of Houston, Houston, TX 77204, USA. E-mail: zren@uh.edu*
[b]*National Center for Nanoscience and Technology, Beijing 100190, China. E-mail: slf@nanoctr.cn*
[c]*School of Physics, State Key Lab for Mesoscopic Physics, Peking University and Collaborative Innovation Center of Quantum Matter, Beijing, China*
† Electronic supplementary information (ESI) available: The experimental details and characterization data. See DOI: 10.1039/c5nr00242g
‡ These authors contributed equally to this work.

electromagnetically enhanced "hot spots" for SERS applications. The enhancement factors depend on the spacing gap:[23] the smaller the gap is, the stronger the enhancement is. However, there is no direct synthesis approach, but only using expensive e-beam lithography (EBL) to pattern gold bowties, with the spacing gap further limited by the system spatial resolution (~8 nm).[23] The advent of two-dimensional layered MoS_2 may fill this gap, which would be an alternative template for growing AuNTs. In this paper, we demonstrated the direct growth and favorable orientation of AuNTs on MoS_2 layers, and aimed to unveil the effect of the number of MoS_2 layers on the AuNT size and areal density. It is interesting to point out that upon heating the substrate, the as-deposited gold adatoms on MoS_2 tend to coalescent into ultrathin equilateral AuNTs, with the particle size and density tuned by the MoS_2 thickness. Few-layer MoS_2 shows better modulation on particle shape than 1L MoS_2, and AuNTs are surprisingly well-oriented on the MoS_2 surface, resulting in the formation of gold bowtie structures with a high density up to 1.6×10^{13} counts per m^2 and interparticle spacing gap down to 3 nm. The AuNTs grow on MoS_2 with $[111]_{Au}||[001]_{MoS_2}$ and $<211>_{Au}||<210>_{MoS_2}$, suggesting that the orientation of AuNTs originates from the lattice epitaxy between MoS_2 and AuNTs. These results indicate that although the MoS_2 interlayer interaction is usually thought to be weak and short ranged, it has a profound effect on modulating the nucleation and growth of AuNTs on the MoS_2 basal plane. Meanwhile, strong Raman enhancements of AuNTs on MoS_2 are observed, which are much stronger than those based on ordinary gold films, indicating the potential use in SERS.

Results and discussion

Thickness determination of pristine *n*-layer MoS_2

Ultrathin MoS_2 sheets were obtained by mechanical cleavage of bulk MoS_2, and transferred onto 300 nm SiO_2/Si substrates.[5,12] The samples were first selected based on their color contrasts under an optical microscope. Fig. 1a and b show typical optical images of the as-prepared monolayer (1L), bilayer (2L), trilayer (3L), quadralayer (4L) and multilayer (ML, $n \geq 5$) MoS_2, from which we can see the different color contrasts among MoS_2 flakes with different thicknesses. After selecting thin MoS_2 sheets, we have applied Raman and PL spectroscopy to further determine the number of MoS_2 layers (Fig. 1c and d). It is noteworthy that the frequency difference between two Raman A_{1g} and E^1_{2g} modes (Fig. 1c) is distinctively different for different number of layers, which increases with the increase of MoS_2 layers. While in the PL spectra (Fig. 1d), the peak intensity of 1L at around 1.84 eV is much more prominent than other *n*-layer MoS_2, which is due to the transition from indirect (few-layer) to direct (1L) band-gap semiconductor. The differences in Raman and PL spectra as a function of thickness are very consistent with previously reported results.[15,24]

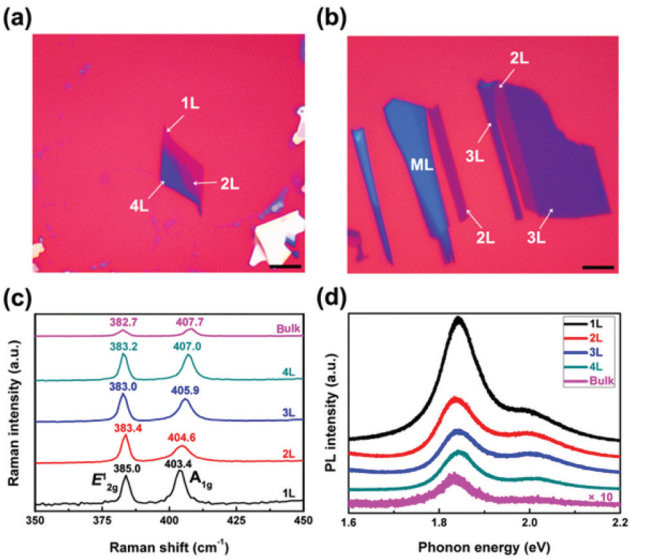

Fig. 1 (a) A representative optical image of 1L, 2L and 4L MoS_2 transferred onto the silicon substrate. (b) An optical image showing the different color contrasts of 2L, 3L and ML MoS_2 on the substrate. Scale bar: 5 μm. (c) and (d) Raman and PL spectra of *n*-layer MoS_2 (n = 1, 2, 3, 4 and bulk) excited by 514.5 nm, respectively.

Epitaxial growth of AuNTs or gold bowties on MoS_2

Although ultrathin MoS_2 sheets show hexagonal layered-lattice crystal structures, 1L MoS_2 is truly different from graphene in that it is composed of three atomic layers: a Mo layer sandwiched between two S layers. These would result in special properties on the few-layer MoS_2 surface. To further demonstrate this point, we have thermally evaporated ultrathin gold films onto the pre-heated MoS_2 surface (ESI†), and investigated the effects of MoS_2 thickness on gold morphologies in detail by using scanning electron microscopy (SEM).

By thermally depositing a thin gold film onto the pre-heated MoS_2 surface, we find that the morphology of gold on MoS_2 is layer dependent (Fig. 2). On the one hand, it is surprising to find that gold adatoms tend to nucleate and grow into AuNTs as shown in Fig. 2a and b, with the particle size modulated by the MoS_2 thickness: the thicker the MoS_2 sheet is, the larger the size of AuNTs is (Fig. S1†). In contrast, no AuNTs can be found on bare SiO_2/Si substrates (Fig. 2a). These triangular structures are consistent with recently published results on the growth of MoS_2 single crystals by the chemical vapor deposition (CVD) method,[12,25] in which single grains tend to grow in triangular shape. The observed triangular shape (Fig. 2) may imply that a special direction of AuNTs is more stable when they are grown on the MoS_2 surface, so as to ensure the smallest surface free energy during growth. Once we deposit a thicker gold film like 4.0 nm, some of the nanoparticles become irregular, and so the effects of MoS_2 thickness on the shape of gold nanostructures become much more prominent (Fig. 2c–e): the AuNPs on 1L MoS_2 are mainly composed of irregular islands, while on thicker MoS_2, like 2L, 3L

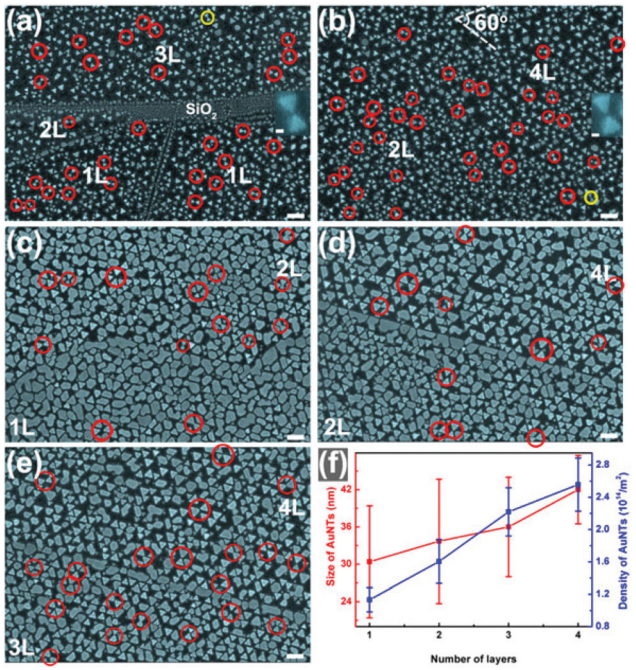

Fig. 2 Typical SEM images showing the growth of ultrathin equilateral AuNTs on *n*-layer MoS_2 with controlled gold film thickness and substrate temperature. (a and b) 2.0 nm at 375 °C. The circles indicate the formation of gold bowties on MoS_2, and the insets show the enlarged sizes of the yellow-marked bowties with 10 nm bar and false color. (c–e) 4.0 nm at 375 °C. (f) The statistical diagram showing the edge length and density of AuNTs as a function of MoS_2 layers as shown in (c)–(e). Scale bar for (a)–(e): 100 nm.

or 4L, more AuNPs exhibit equilateral triangular shape, indicating that 1L MoS_2 is not so suitable for nanotriangle formation compared with other few-layer MoS_2 under the same conditions. In particular, with the increase of MoS_2 thickness, the density of AuNTs becomes much higher, and the size gradually increases (Fig. 2c–e), making it evident that AuNTs are preferentially grown on few-layer rather than on 1L MoS_2, and the growth of triangular AuNPs is truly related to the MoS_2 thickness. To account for the thickness dependence of gold morphologies on the number of MoS_2 layers, we need to consider the nucleation and growth of gold adatoms on the MoS_2 surface, which is determined by the thickness-dependent surface diffusion coefficient and barrier caused by the interlayer interactions as in the situation of gold on the graphene surface.[5,7] Meanwhile, it is apparent from the images (Fig. 2a–e) that the deposited Au atoms have the tendency to aggregate at MoS_2 edges or at terraced edges where MoS_2 flakes stack together, which is probably attributed to the reason that Au atoms have larger binding energy with the edge Mo/S atoms than that at the central regions. For instance, the AuNPs are nearly connected with each other at the terraced edges between 2L and 4L (Fig. 2d), or 3L and 4L MoS_2 (Fig. 2e), indicating the aggregation of gold atoms at these border lines.

To the best of our knowledge, it is probably the first time gold bowties are directly synthesized on MoS_2 templates without using the lithography method. As shown in Fig. 2a and b, it is worth mentioning that lots of bowtie structures (marked with red circles in Fig. 2a and b) consist of two nanotriangles with tips facing each other for gaps as small as 3 nm (the insets of Fig. 2a and b), which is much smaller than the reported value, and the relevant density can be up to 1.6×10^{13} counts per m^2. Meanwhile, the gap in the gold bowties is in the range of 3–10 nm, and most of the gaps are around 4–6 nm (Fig. S2†). In addition, the size of gold bowties is closely related to the gold film thickness, and can be tuned through changing the film thickness (Fig. 2). With the increase of film thickness from 2 nm to 4 nm, the edge lengths of AuNTs range from ~20 nm to 40 nm, resulting in the formation of gold bowties with larger spatial size. Finally, we find that the areal density of gold bowties increases with the increase of the density of AuNTs.

Lattice epitaxy between MoS_2 and AuNTs

To gain further insights into the effects of MoS_2 on the nucleation and growth of equilateral AuNTs, we carried out HRTEM observation to characterize the structural relationship between gold and MoS_2 (Fig. 3). The oriented nanotriangles are epitaxially grown on MoS_2. Au has a face-centered cubic (fcc) crystal structure, which is six-fold-symmetric along the [111]-axis,

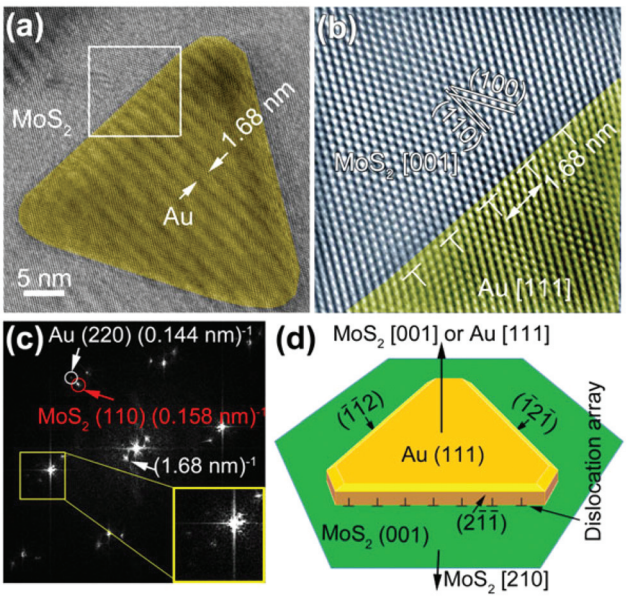

Fig. 3 Epitaxial growth of Au nanotriangles. (a) HRTEM image of a AuNT on MoS_2. (b) Fourier filtered image of the white square in panel (a), showing a dislocation array with a spacing of 1.68 nm at the boundary of the Au triangle. (c) Fourier transformation pattern of the Au triangle, indicating that Au triangles are grown on MoS_2 with $\{220\}_{Au}||\{110\}_{MoS_2}$. The diffraction spots in the yellow square exhibit a six-fold symmetry of the dislocations. (d) Schematic of the structural relationship between Au and MoS_2. Note that there are three dislocation arrays that are perpendicular to the $(2\bar{1}\bar{1})$, $(\bar{1}2\bar{1})$ and $(\bar{1}\bar{1}2)$ facets of the AuNT, respectively.

while MoS_2 has a hexagonal structure and is also six-fold-symmetric along the [001]-axis. Although the lattice mismatch

$$f = \frac{d_{Au\{220\}} - d_{MoS_2\{110\}}}{d_{MoS_2\{110\}}} \quad (1)$$

between these two materials is large (8.8% between Au {220} and MoS_2 {110}, with a *d*-spacing of 0.144 nm and 0.158 nm, respectively), the AuNTs can grow on the MoS_2 surface by introducing dislocation arrays with a pitch of ~1.68 nm to form stress-free interfaces. That is, dislocations appear every 11.6 Au {220} spacings or every 10.6 MoS_2 {110} spacings. Similar epitaxial growth has been reported in other systems with a large lattice misfit, like Zn/ZnO nanostructures.[26] Fig. 3a shows a representative HRTEM image of Au nanotriangles on MoS_2 with 1.68 nm-pitch Moiré fringes. Each Moiré fringe represents a misfit dislocation at the Au/MoS_2 interface. Fig. 3b exhibits the dislocations along the [211]-directions of Au or the [2$\bar{1}$0]-directions of MoS_2. Due to the six-fold symmetry of both materials, there are three dislocation arrays with an intersection angle of 120° at the Au/MoS_2 interface. Probably due to the fact that the HRTEM image was not exactly obtained from the [001] zone axis of MoS_2, we can only see one set of Moiré fringes perpendicular to one edge of the nanotriangle. However, we can find the six-fold symmetry of the Moiré fringes by analyzing the Fourier transformation pattern of the TEM image, as shown in the yellow square in Fig. 3c. We also show a schematic (Fig. 3d) that explains the structural relationship between the AuNT and the underlying MoS_2. And, we predict that such a formation mechanism of AuNTs on MoS_2 may govern the growth of other metals with a fcc structure (*e.g.*, Ag, Cu, Ni, and Al) or a hexagonal structure (*e.g.*, Zn), enabling much wider applications. However, for different metals the distance between neighboring dislocations differs as a result of the changed extent of lattice misfit.

Highly-improved Raman enhancement

To search for the possible applications of this kind of MoS_2-based composites, we have used Raman spectroscopy to investigate the SERS properties of well-oriented AuNTs (Fig. 4). The micro-Raman spectroscopy (Renishaw inVia Raman Spectroscope) experiments were performed under ambient conditions with a 785 nm (1.58 eV) laser. All the spectra were collected under the same ambient conditions (laser power, exposure time, *etc.*). As shown in Fig. 4a and b, it is clearly seen that Raman signals of as-fabricated MoS_2 samples are almost undetectable at 785 nm laser excitation. When a 2 nm gold film is deposited onto the MoS_2 surface at room temperature, we can detect the Raman signal with the Raman peaks appearing clearly, however, the signal is relatively weak. In contrast, if *n*-layer MoS_2 is fully covered by AuNTs prepared by our method, the Raman signals of 1L or 2L MoS_2 are greatly enhanced, indicating that triangular AuNPs can efficiently enhance Raman scattering of *n*-layer MoS_2 compared with ordinary gold particles. This could be attributed to the sharp corners in a nanotriangle, where electromagnetic fields are

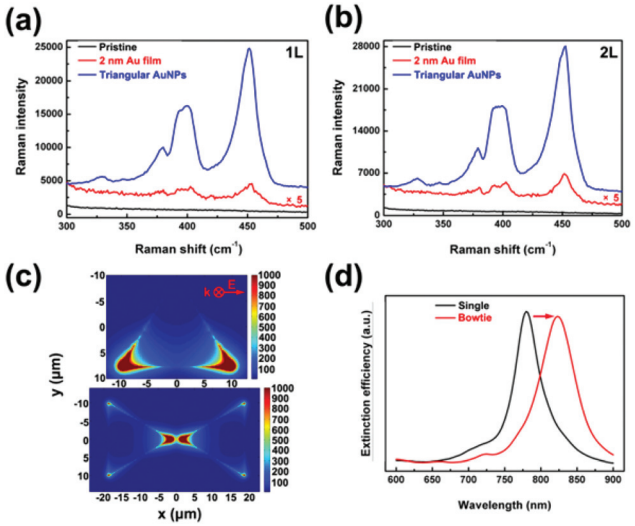

Fig. 4 The comparison among the Raman spectra of original MoS_2, gold film-deposited on MoS_2 and ultrathin AuNTs decorated on 1L (a) and 2L (b) MoS_2 excited by a 785 nm laser. (c) The electromagnetic field enhancement contour external to an individual AuNT and bowtie with a 2 nm thickness and 20 nm edge length at a 785 nm laser excitation. (d) The calculated extinction spectrum of a nanotriangle and relevant bowtie structure with a spacing gap of 3 nm.

concentrated into "hot-spots", thus resulting in strong Raman enhancements on the Raman signals of MoS_2.[21,27] In order to figure out the physical origins, we have carried out theoretical simulations (ESI†). Indeed, according to the electromagnetic field contour (Fig. 4c), there is a very strong field enhancement at the sharp edges of a nanotriangle or a bowtie structure. In particular, by examining the relevant extinction spectrum, we can note that there is a strong in-plane dipole plasmon resonance at 785 nm in an AuNT (black in Fig. 4d), while for gold bowties, their extinction spectra also show prominent resonant peaks close to 785 nm (red in Fig. 4d and Fig. S4, ESI†), suggesting the contribution of single AuNT or bowties to the Raman enhancement arising from the coupled surface plasmon resonance absorption. These results would further boost the application of MoS_2-based metal composites possibly in SERS.

Conclusions

In summary, we reported here, the nucleation and growth of equilateral triangular AuNPs on layered MoS_2 with well-defined crystallographic orientations, and an average size controlled by the MoS_2 thickness, suggesting thickness-dependent interactions and the epitaxial growth of Au on *n*-layer MoS_2. Our technique is of great potential for direct synthesis of gold bowtie nanoantennas where two AuNTs opposing tip to tip with the gap as small as 3 nm, which is far below the spatial resolution of e-beam lithography (~8 nm). In particular, these well-oriented AuNTs exhibit excellent Raman enhancing effects, indicating the potential application of AuNTs for molecule detection.

Acknowledgements

This project was partially supported by the National Natural Science Foundation of China (Grant no. 10774032, 51472057, 61422501 and 11374023), the National Basic Research Program of China (973 Program) (Grant no. 2015CB932400), the Beijing Natural Science Foundation (Grant no. L140007), and partially by the US Defense Threatening Reduction Agency (DTRA) under grant FA 7000-13-1-0001.

Notes and references

1 K. S. Novoselov, A. K. Geim, S. V. Morozov, D. Jiang, Y. Zhang, S. V. Dubonos, I. V. Grigorieva and A. A. Firsov, *Science*, 2004, **306**, 666–669.
2 K. S. Novoselov, D. Jiang, F. Schedin, T. J. Booth, V. V. Khotkevich, S. V. Morozov and A. K. Geim, *Proc. Natl. Acad. Sci. U. S. A.*, 2005, **102**, 10451–10453.
3 Q. H. Wang, K. Kalantar-Zadeh, A. Kis, J. N. Coleman and M. S. Strano, *Nat. Nanotechnol.*, 2012, **7**, 699–712.
4 Z. Liu, L. Song, S. Z. Zhao, J. Q. Huang, L. L. Ma, J. N. Zhang, J. Lou and P. M. Ajayan, *Nano Lett.*, 2011, **11**, 2032–2037.
5 H. Q. Zhou, C. Y. Qiu, Z. Liu, H. C. Yang, L. J. Hu, J. Liu, H. F. Yang, C. Z. Gu and L. F. Sun, *J. Am. Chem. Soc.*, 2010, **132**, 944–946.
6 Z. T. Luo, L. A. Somers, Y. P. Dan, T. Ly, N. J. Kybert, E. J. Mele, *et al.*, *Nano Lett.*, 2010, **10**, 777–781.
7 H. Q. Zhou, F. Yu, M. J. Chen, C. Y. Qiu, H. C. Yang, G. Wang, T. Yu and L. F. Sun, *Carbon*, 2013, **52**, 379–387.
8 K. F. Mak, C. Lee, J. Hone, J. Shan and T. F. Heinz, *Phys. Rev. Lett.*, 2010, **105**, 136805.
9 J. R. Lince, D. J. Carre and P. D. Fleischauer, *Phys. Rev. B: Condens. Matter*, 1987, **36**, 1647.
10 T. S. Sreeprasad, P. Nguyen, N. Kim and V. Berry, *Nano Lett.*, 2013, **13**, 4434.
11 S. Najmaei, Z. Liu, W. Zhou, X. L. Zou, G. Shi, S. D. Lei, B. I. Yakobson, J. C. Idrobo, P. M. Ajayan and J. Lou, *Nat. Mater.*, 2013, **12**, 754–759.
12 H. Q. Zhou, F. Yu, Y. Y. Liu, X. L. Zou, C. X. Cong, C. Y. Qiu, T. Yu, Z. Yan, X. N. Shen, L. F. Sun, B. I. Yakobson and J. M. Tour, *Nano Res.*, 2013, **6**, 703–711.
13 S. Helveg, J. V. Lauritsen, E. Lægsgaard, I. Stensgaard, J. K. Nørskov, B. S. Clausen, H. Topsøe and F. Besenbacher, *Phys. Rev. Lett.*, 2000, **84**, 951.
14 B. Radisavljevic, A. Radenovic, J. Brivio, V. Giacometti and A. Kis, *Nat. Nanotechnol.*, 2011, **6**, 147–150.
15 A. Splendiani, L. Sun, Y. B. Zhang, T. S. Li, J. Kim, C. Y. Chim, G. Galli and F. Wang, *Nano Lett.*, 2010, **10**, 1271–1275.
16 T. S. Sreeprasad, P. Nguyen, N. Kim and V. Berry, *Nano Lett.*, 2013, **13**, 4434–4441.
17 M. W. Knight, H. Sobhani, P. Nordlander and N. J. Halas, *Science*, 2011, **332**, 702–704.
18 L. Scarabelli, M. Coronado-Puchau, J. J. Giner-Casares, J. Langer and L. M. Liz-Marzán, *ACS Nano*, 2014, **8**, 5833–5842.
19 D. A. Walker, K. P. Browne, B. Kowalczyk and B. A. Grzybowski, *Angew. Chem., Int. Ed.*, 2010, **49**, 6760–6763.
20 P. R. Sajanlal and T. Pradeep, *Adv. Mater.*, 2008, **20**, 980–983.
21 A. Kinkhabwala, Z. F. Yu, S. H. Fan, Y. Avlasevich, K. Müllen and W. E. Moerner, *Nat. Photonics*, 2009, **3**, 654–657.
22 N. Liu, M. L. Tang, M. Hentschel, H. Giessen and A. P. Alivisatos, *Nat. Mater.*, 2011, **10**, 631–636.
23 N. A. Hatab, C. Hsueh, A. Gaddis, S. Retterer, J. H. Li, G. Eres, Z. T. Zhang and B. H. Gu, *Nano Lett.*, 2010, **10**, 4952–4955.
24 C. G. Lee, H. G. Yan, L. E. Brus, T. F. Heinz, J. Hone and S. Ryu, *ACS Nano*, 2010, **4**, 2695–2700.
25 A. M. van der Zande, P. Y. Huang, D. A. Chenet, T. C. Berkel-bach, Y. M. You, G. H. Lee, T. F. Heinz, D. R. Reichman, D. A. Muller and J. C. Hone, *Nat. Mater.*, 2013, **12**, 554–561.
26 C. F. Guo, Y. Wang, P. Jiang, S. Cao, J. Miao, Z. Zhang and Q. Liu, *Nanotechnology*, 2008, **19**, 445710.
27 P. J. Schuck, D. P. Fromm, A. Sundaramurthy, G. S. Kino and W. E. Moerner, *Phys. Rev. Lett.*, 2005, **94**, 017402.